tiplicities along a period[3a] as well as variations in the participation[3c] from the $(n + 1)$s orbital in the M-R bond down a triad.[3c]

Our calculated bond strengths are in fair agreement with the few available experimental data on D(M-R) bond energies in RML_n complexes. Connor[4c] et al. found for $RMn(CO)_5$ that D(Mn-H) = 213 kJ mol^{-1} and D(Mn-CH_3) = 153 kJ mol^{-1}, respectively. Ungvary[4d] has further measured D(H-$Co(CO_4)$) as 238 kJ mol^{-1}, in close accord with our theoretical value of 230 kJ mol^{-1}. We expect the upper bound for the errors in the calculated M-H and M-CH_3 bond energies to be 50 kJ mol^{-1}. The errors in the calculated relative strengths of the M-H and M-CH_3 bonds should however be less.

Concluding Remarks

The main objective in the present investigation has been to reveal the factors governing the general periodic trends in relative M-H and M-CH_3 bond strengths across a transition series. We have found that the M-CH_3 bond is considerably weaker than the M-H bond for late to middle transition metals as a result of the repulsive interaction between the fully occupied (mainly) $2s_c$ orbital on CH_3 and the σ-bonding CH_3ML_n orbital ϕ_σ, where ϕ_σ is an in-phase combination between the singly occupied $2\sigma_{Me}$ and σ_{ML} orbitals on CH_3 and ML_n, respectively. The repulsive interaction between the fully occupied (mainly) $2s_c$ orbital on CH_3 and ϕ_σ is reduced in methyl complexes of early transition metals due to the high polarity of the M-CH_3 bond, with the result that M-H and M-CH_3 bonds become comparable in strength. The intrinsic M-H bond energy D(M-H) does not change noticeably across a transition series. The M-H bond as well as the M-CH_3 bond are strengthened on decending a triad due to an increase in the bonding overlap between $2\sigma_{Me}$ and σ_{ML}.

We do not expect that the main conclusions reached here will be changed by more accurate calculations including extensive geometry optimization. Studies are now under way on the relative M-H and M-CH_3 bond strengths in complexes of f-block elements. A comparison between M-H and M-L bond strengths for a number of one-electron ligands L, which in analogy with CH_3 have a singly occupied $2\sigma_L$ orbital and a fully occupied $1\sigma_L$ orbital, is given in ref 6.

Acknowledgment. This investigation was supported by the Natural Sciences and Engineering Research Council of Canada (NSERC). We also acknowledge access to the Cyber-205 installations at the University of Calgary and SARA in Amsterdam. The research of W.R. has been made possible by a (Senior) fellowship from the Royal Netherlands Academy of Arts and Sciences.

Registry No. Cp_2ScH, 116301-38-3; Cp_2ScCH_3, 116301-39-4; Cp_2VH, 116301-40-7; Cp_2VCH_3, 54111-39-6; Cp_2MnH, 116301-41-8; Cp_2MnCH_3, 116301-42-9; Cp_2YH, 116301-43-0; Cp_2LaH, 116301-44-1; Cp_2TcH, 12116-92-6; Cp_2ReH, 1271-32-5; Cp_2YCH_3, 116301-45-2; Cp_2LaCH_3, 116301-46-3; Cp_2TcCH_3, 116301-47-4; Cp_2ReCH_3, 72316-82-6; $CpNi(CO)H$, 116301-48-5; $CpFe(CO)_2H$, 35913-82-7; $CpCr(CO)_3H$, 36495-37-1; $CpNi(CO)CH_3$, 92476-37-4; $CpFe(CO)_2CH_3$, 12080-06-7; $CpCr(CO)_3CH_3$, 41311-89-1.

Contribution from the Department of Chemistry, University of California, Santa Barbara, California 93106

Synthesis, Structure, Electrochemistry, and Photophysics of Methyl-Substituted Phenylpyridine Ortho-Metalated Iridium(III) Complexes

F. O. Garces, K. A. King, and R. J. Watts*

Received August 26, 1987

Synthetic, structural, photophysical, and electrochemical characterizations of ortho-metalated $[Ir(NC)_2Cl]_2$ dimeric and $[Ir(NC)_2NN]Cl$ monomeric complexes, where NC = 2-(*p*-tolyl)pyridine (ptpy) or 3-methyl-2-phenylpyridine (mppy) and NN = 2,2'-bipyridine (bpy), are described. Structural characterizations by ^1H and ^{13}C nuclear magnetic resonance (NMR) indicate the presence of symmetry elements in these complexes. Proton resonances were assigned by two-dimensional homonuclear *J*-correlation spectroscopy (2D-COSY), and carbon resonances were elucidated by single-frequency off-resonance decoupling (SFORD) and attached proton test (APT) experiments. NMR data support a structural configuration for these complexes in which the Ir-N bonds from the pyridyl rings of the metalating ligands (i.e., ptpy, mppy) are mutually trans. The ultraviolet-visible absorption properties of these complexes are similar to those of the nonsubstituted phenylpyridine (ppy) complexes, with the dimers showing low-energy charge-transfer bands ranging from 484 to 400 nm and the monomers displaying charge-transfer transitions ranging from 468 to 325 nm. The emission spectra are also similar to those of the nonsubstituted ppy complexes; at room temperature the dimers show broad emission bands at 515 nm, and in 77 K glasses they show structured emissions at 494 and 528 nm. The emission spectra of the monomers indicate dual emissive states, as has been suggested for the nonsubstituted $[Ir(ppy)_2bpy]^+$ monomer. At room temperature in fluid solvents, an emission maximum is centered at 595 nm, but at low temperatures (77 K glasses), structured emissions with maxima centered at 527 and 550 nm are observed. Emission lifetimes are in the range 32-250 ns under ambient conditions and range from 4.4 to 5.2 μs at 77 K. Cyclic voltammetric measurements reveal that these methyl-substituted complexes are easier to oxidize and harder to reduce relative to the nonsubstituted ppy complexes. Cathodic shifts in the half-wave potentials ($\sim$100 mV) compared to the potential of the ppy complex suggest that the electron density around the iridium metal, which influences the reducing power of these complexes, may be controlled via inductive effects from the methyl group on the phenylpyridine ligands.

I. Introduction

Transition-metal complexes containing ligands with extended π-systems (e.g., pyridine, bipyridine) have generated tremendous interest because of their potential to participate as photocatalysts in solar-driven artificial photoconversion processes.[1-10] The classic example of a molecule used as a photocatalyst in photoconversion systems is $Ru(bpy)_3^{2+}$.[3,4,5,11-15] The excited-state redox potentials of metal complexes such as $Ru(bpy)_3^{2+}$ may be altered by several types of structural modifications. Potential modifications include (i) changing the central metal, (ii) replacing some or all of the

(1) Kirch, M.; Lehn, J.-M.; Sauvage, J.-P. *Helv. Chim. Acta* **1979**, *62*, 1345.
(2) Lehn, J.-M. In *Photochemical Conversion and Storage of Solar Energy*; Connolly, J. S., Ed.; Academic: New York, 1981; Chapter 6.
(3) Kalyanasundaram, K. *Coord. Chem. Rev.* **1982**, *46*, 159.
(4) Kutal, C. *J. Chem. Educ.* **1983**, *60*(10), 882.
(5) Scandola, F.; Balzani, V. In ref 2, Chapter 4.
(6) Sutin, N.; Creutz, C. *Acc. Chem. Res.* **1968**, *1*, 225.
(7) Meyer, T. J. *Acc. Chem. Res.* **1978**, *11*, 94.
(8) Sutin, N.; Creutz, C. *J. Chem. Educ.* **1983**, *60*, 809.
(9) Balzani, V.; Scandola, F. In ref 2, Chapter 4.
(10) Adamson, A. W. *J. Chem. Educ.* **1983**, *60*, 797.
(11) Balzani, V.; Bolletta, F.; Gandolfi, M. T.; Maestri, M. *Top. Curr. Chem.* **1978**, *75*, 1.
(12) Sutin, N.; Creutz, C. *Adv. Chem. Ser.* **1977**, *No. 168*, 1.
(13) Watts, R. J. *J. Chem. Educ.* **1983**, *60*, 834.
(14) Launikonis, A.; Lay, P. A.; Mau, A. W.-H.; Sargeson, A. M.; Sasse, W. H. F. *Aust. J. Chem.* **1986**, *39*, 1053.
(15) Sabbatini, N.; Dellonte, S.; Bonazzi, A.; Ciano, M.; Balzani, V. *Inorg. Chem.* **1986**, *25*, 1738.

0020-1669/88/1327-3464$01.50/0

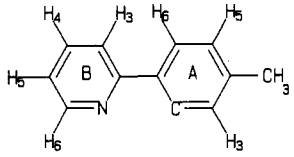

(a) ptpy

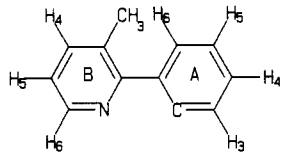

(b) mppy

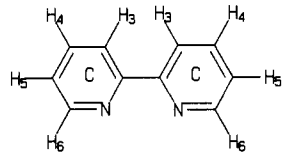

(c) bpy

Figure 1. Ortho-metalating and chelating ligands: (a) NC = 2-(*p*-tolyl)pyridine (ptpy); (b) NC = 3-methyl-2-phenylpyridine (mppy); (c) NN = 2,2′-bipyridine (bpy).

ligands with other suitable ligands, (iii) modifying the ligands by adding suitable functional groups, and (iv) using mixed-bimetallic complexes to access, within a single chemical moiety, redox properties associated with each monomeric complex. Changing the metal in $Ru(bpy)_3^{2+}$ to Ir(III), for example, produces a complex, $Ir(bpy)_3^{3+}$, with excellent photooxidizing power (~2 V).[16] On the other hand, replacing bpy in $Ir(bpy)_3^{3+}$ by 2-phenylpyridine (ppy) produces a very strong photoreductant, $Ir(ppy)_3$.[17] Species containing both bpy and ppy coordinated to a common metal ion center, such as $[Ir(ppy)_2bpy]^+$, have intermediate photoredox capabilities and can operate as either photooxidants or photoreductants.[18] Thus, the optimization of photoredox properties of metal complexes can be provided by the combination of ortho-metalating ligands such as ppy and its derivatives with coordinating ligands such as bpy.

Ortho-metalation reactions of the type used in preparation of ppy complexes are common in the literature, and many of the products have been well characterized.[19-24] For example, the major complex produced in reactions of Ir(III) with ppy is an ortho-metalated dimer, $[Ir(ppy)_2Cl]_2$, which, like the triply ortho-metalated ppy monomer, is also a powerful photoreducing agent.[25] The enhanced photoreducing potential of these ortho-metalated complexes is attributed to the increase of electron density about the metal due to the strong σ-donor character of the coordinating carbon, which facilitates electrochemical oxidation at the metal center as evidenced in electrochemical measurements.[26] Furthermore, low-energy metal-to-ligand charge-transfer transitions result when both σ-metalating ligands such as ppy and good π-accepting ligands such as bpy are present in the coordination sphere of a central metal ion as in $[Ir(ppy)_2bpy]^+$.[18,26]

The purpose of this work was to explore the enhancement of the already high photoreducing potential of ortho-metalated complexes such as $[Ir(ppy)_2Cl]_2$ and $[Ir(ppy)_2bpy]^+$ by introducing

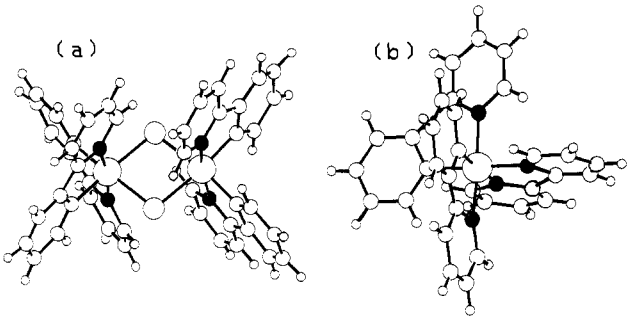

Figure 2. CHEM-X representative structures of Ir(III) parent complexes: (a) $[Ir(ppy)_2Cl]_2$; (b) $[Ir(ppy)_2bpy]^+$. The corresponding methyl-substituted complexes are obtained by replacing ppy with either ptpy or mppy.

functional groups onto the ppy ligand. Two ortho-metalating ligands employed for this purpose were 3-methyl-2-phenylpyridine (mppy) and 2-(*p*-tolyl)pyridine (ptpy) (see Figure 1). These ligands contain activating methyl groups, which donate electron density to either the phenyl ring (ptpy) or the pyridyl ring (mppy). The results of a study of Ir(III) complexes containing methyl-substituted ortho-metalating ligands (see Figure 2) are reported here.

II. Experimental Section

A. Synthesis. Tetrakis(2-(*p*-tolyl)pyridine-C^2,N)bis(μ-chloro)diiridium. Iridium trichloride hydrate (0.3557 g, 1.0 mmol) was combined with 2-(*p*-tolyl)pyridine (0.70 mL, 4.4 mmol) in 2-ethoxyethanol (30 mL, distilled and dried over $MgSO_4$) and water (10 mL). The preparation and purification of this complex were carried out analogously to the $[Ir(ppy)_2Cl]_2$ synthesis.[19,25] The resulting dark yellow crystals and the yellow amorphous powder were collected on a glass frit and dried to yield the product (0.148 g, 26.22%). Anal. Calcd for $Ir_2C_{48}H_{40}N_4Cl_2 \cdot {}^3/_4C_7H_8$: C, 53.42; H, 3.87; N, 4.68; Cl, 5.92. Found: C, 53.29; H, 3.90; N, 4.52.

Tetrakis(3-methyl-2-phenylpyridine-C^2,N)bis(μ-chloro)diiridium. The synthesis and workup of this product, using iridium trichloride hydrate (0.3527 g, 1.0 mmol) and 3-methyl-2-phenylpyridine (0.70 mL, 4.4 mmol), was carried out analogously to the $[Ir(ptpy)_2Cl]_2$ synthesis to give $[Ir(mppy)_2Cl]_2$ as a bright yellow amorphous powder (0.2829 g, 50.16%). Anal. Calcd for $Ir_2C_{48}H_{40}N_4Cl_2$: C, 51.10; H, 3.57; N, 4.97; Cl, 5.74. Found: C, 50.78; H, 3.66; N, 4.62.

(2,2′-Bipyridine)bis(2-(*p*-tolyl)pyridine)iridium(III) Chloride. The iridium 2-(*p*-tolyl)pyridine dichloro-bridged dimer (55.0 mg, 0.049 mmol) in dichloromethane (4.0 mL) was added to a mixture of 2,2′-bipyridine (22.2 mg, 0.14 mmol) in dichloromethane (1.0 mL). The preparation of this complex was carried out analogously to the $[Ir(ppy)_2bpy]Cl$[18,26] synthesis to give an amorphous yellow powder of the $[Ir(ptpy)_2bpy]Cl$ mononer (66.9 mg, 92.5%).

(2,2′-Bipyridine)bis(3-methyl-2-phenylpyridine)iridium(III) Chloride. The synthesis and workup of this product, using the iridium 3-methyl-2-phenylpyridine dichloro-bridged dimer (54.3 mg, 0.048 mmol) and bipyridine (22.2 mg, 0.14 mmol), was carried out analogously to the $[Ir(ptpy)_2bpy]Cl$ synthesis to give $[Ir(mppy)_2bpy]Cl$ as an amorphous yellow powder (70.0 mg, 90.3%).

B. Measurements. Absorption spectra were obtained with a Cary 15 spectrophotometer. Dimer samples were generally dissolved in dichloromethane with monomer samples dissolved in acetonitrile; the concentration ranged from 10^{-4} to 10^{-6} M.

^1H NMR spectra were obtained with a Nicolet NT-300 FT NMR spectrometer, although it was necessary to use a General Electric GN-500 FT NMR spectrometer for the ^{13}C NMR spectra to obtain satisfactory resolution. Dimer samples were dissolved in dichloromethane-d_2 and monomer samples were dissolved in acetonitrile-d_3, dichloromethane-d_2, or chloroform-d for analysis. Two-dimensional homonuclear J-correlation spectroscopy (2D-COSY) experiments were instrumental in proton assignments of these complexes while single-frequency off-resonance decoupling (SFORD) and attached proton test (APT) experiments helped elucidate the ^{13}C NMR spectra.

An IBM EC-225 voltammetric analyzer was used to obtain cyclic voltammogram (CV) measurements for these complexes. Room-temperature CV's with tetraethylammonium hexafluorophosphate (TEAH) supporting electrolyte were obtained in either dichloromethane (distilled and dried over $CaCl_2$) for dimer samples or acetonitrile (distilled and dried over CaH_2) for monomer samples. TEAH (1.0 g) and alumina (0.5 g) in 50 mL of solvent (degassed with dry dinitrogen) were used for the electrolyte solution. Low-temperature measurements (196 K) required

(16) Bergeron, S. F.; Watts, R. J. *J. Am. Chem. Soc.* **1979**, *101*, 3151.
(17) King, K. A.; Spellane, P. J.; Watts, R. J. *J. Am. Chem. Soc.* **1985**, *107*, 1431.
(18) King, K. A.; Watts, R. J. *J. Am. Chem. Soc.* **1987**, *109*, 1589.
(19) Nonoyama, M.; Yamasaki, K. *Inorg. Nucl. Chem. Lett.* **1971**, *7*, 943.
(20) Nonoyama, M. *Bull. Chem. Soc. Jpn.* **1974**, *47*, 767.
(21) Dehand, J.; Pfeffer, M. *Coord. Chem. Rev.* **1976**, *18*, 327.
(22) Omae, I. *Chem. Rev.* **1979**, *79*, 287.
(23) Selbin, J.; Gutierrez, M. A. *J. Organomet. Chem.* **1981**, *214*, 253.
(24) Newkome, G. R.; Puckett, W. E.; Gupta, V. K.; Kiefer, G. E. *Chem. Rev.* **1986**, *86*, 451.
(25) Sprouse, S. D.; King, K. A.; Spellane, P. J.; Watts, R. J. *J. Am. Chem. Soc.* **1984**, *106*, 6647.
(26) Ohsawa, Y.; Sprouse, S. D.; King, K. A.; DeArmond, M. K.; Hanck, K. W.; Watts, R. J. *J. Phys. Chem.* **1987**, *91*, 1047.

Table I. Absorption Data for Ir(III) Dimers and Monomers of ppy, ptpy, and mppy in Dichloromethane

complex	abs feature, nm	$10^{-3}\epsilon$, M^{-1} cm^{-1}
$[Ir(ppy)_2Cl]_2$	484 (sh)	1.1
	434	4.2
	400	6.3
	355 (sh)	11.0
	335	13.0
	260	68.0
$[Ir(ptpy)_2Cl]_2$	482	1.0
	430	4.5
	400	6.4
	355 (sh)	11.3
	310 (sh)	35.4
	280 (sh)	56.5
	263	73.3
$[Ir(mppy)_2Cl]_2$	484 (sh)	1.4
	437	5.0
	400	7.1
	355 (sh)	13.9
	337	16.4
	300	36.5
	270	68.6
$[Ir(ppy)_2bpy]^+$	465	0.58
	410	2.8
	375	4.7
	335 (sh)	
	310	16.1
	265	36.1
$[Ir(ptpy)_2bpy]^+$	468	0.71
	411 (sh)	4.03
	380	6.6
	325 (sh)	12.8
	314 (sh)	20.9
	273	45.9
	258	42.6
$[Ir(mppy)_2bpy]^+$	467	0.87
	416 (sh)	4.41
	382	6.82
	363 (sh)	7.2
	340	10.3
	311 (sh)	29.8
	266	47.9
	255	52.4

a dry-ice–acetone bath for the CV cell. Background voltammograms were first determined for each complex by running CV's of the electrolyte solution, after which approximately 2 mg of the complex was added to the working cell chamber and the CV was recorded. In some instances, current sensitivity and switching potentials were varied to elucidate wave patterns in the voltammograms. After the voltammograms were measured for each complex, voltammograms were measured for ferrocene (5.0 mg). For discussion purposes, the redox potentials for these complexes are referenced to the standard calomel electrode (SCE), but when relative redox potentials are compared, measurements are made relative to the ferrocenium/ferrocene couple ($Fc^{+/0}$).

Luminescence lifetimes were determined by an Avco C950 nitrogen laser with 337-nm pulses. Emission spectral data at room and low temperatures (77 K) were obtained with a Perkin-Elmer MPF-3 spectrophotofluorimeter or a Spex Fluorolog 2 series spectrophotometer. Dichloromethane solvent was used for both dimer and monomer ambient-temperature emission measurements. Under 77 K glass conditions, the dimers were dissolved in ethanol–methanol–dichloromethane (4:1:1 v/v) and the monomers were dissolved in ethanol–methanol (4:1 v/v).

III. Results

A. Iridium Dimers. 1. Absorption and Emission Properties. Extinction coefficients for absorption maxima of $[Ir(ptpy)_2Cl]_2$ and $[Ir(mppy)_2Cl]_2$ in dichloromethane (Figure 3) are compiled in Table I. Beer's law behavior was followed over the concentration range from 10^{-4} to 10^{-6} M. The emission band maxima from the luminescence spectra of $[Ir(ptpy)_2Cl]_2$ and $[Ir(mppy)_2Cl]_2$ (Figure 3) are compiled in Table II. Room-temperature luminescence lifetimes in both dichloromethane and toluene solvent systems were 140 ns for $[Ir(ptpy)_2Cl]_2$ and 40 ns for $[Ir(mppy)_2Cl]_2$; low-temperature (77 K) lifetimes were 5.0

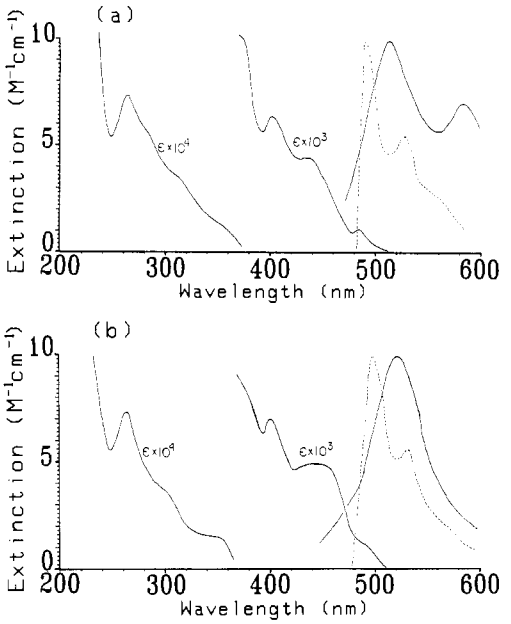

Figure 3. Absorption and emission measurements of Ir(III) dimer complexes (a) $[Ir(ptpy)_2Cl]_2$ and (b) $[Ir(mppy)_2Cl]_2$: (—) absorption and emission at room temperature in CH_2Cl_2; (- - -) emission at 77 K in EtOH–MeOH–CH_2Cl_2 (4:1:1 v/v).

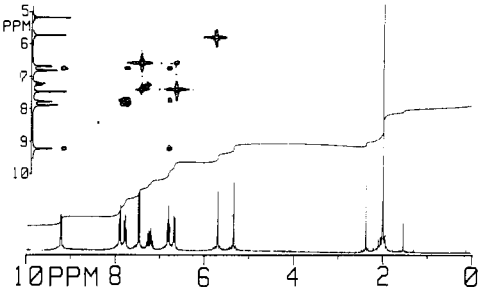

Figure 4. ^1H and 2D-COSY (inset) NMR spectra for $[Ir(ptpy)_2Cl]_2$ in CD_2Cl_2.

Table II. Emission and Lifetime Data for Ir(III) Dimers and Monomers of ppy, ptpy, and mppy

complex	emissn feature, nm	excitn, nm	lifetime, ns
	Room Temperature		
$[Ir(ppy)_2Cl]_2$	518[a]	360	140[a]
$[Ir(ptpy)_2Cl]_2$	510, 580[a]	430, 450	148.8[a]
			133.3[b]
$[Ir(mppy)_2Cl]_2$	520[a]	360	60.3[a]
			32.2[b]
$[Ir(ppy)_2bpy]^+$	606[c]	380	337.5[d]
$[Ir(ptpy)_2bpy]^+$	596[a]	380	248.5[d]
$[Ir(mppy)_2bpy]^+$	594[a]	380	199.7[d]
	Low Temperature (77 K)		
$[Ir(ppy)_2Cl]_2$	483, 525[e]	360	4.0×10^3[f]
$[Ir(ptpy)_2Cl]_2$	490, 526[e]	340, 450	5.2×10^3[f]
$[Ir(mppy)_2Cl]_2$	497, 530[e]	360	5.0×10^3[f]
$[Ir(ppy)_2bpy]^+$	532[f]	360	5.24×10^3[f]
$[Ir(ptpy)_2bpy]^+$	526, 548[f]	360	4.93×10^3[f]
$[Ir(mppy)_2bpy]^+$	528, 551[f]	360	4.38×10^3[f]

[a] Solvent neat dichloromethane. [b] Solvent neat toluene. [c] Solvent neat methanol. [d] Solvent neat acetonitrile. [e] In EtOH–MeOH–DCM (4:1:1 v/v) glass. [f] In EtOH–MeOH (4:1 v/v) glass.

μs for both complexes in EtOH–MeOH (4:1 v/v) (Table II).

2. ^1H and ^{13}C NMR Spectra. The aromatic region in the ^1H NMR spectra of $[Ir(ptpy)_2Cl]_2$ (Figure 4) and $[Ir(mppy)_2Cl]_2$ is integrated for seven resonances (excluding CD_2Cl_2 solvent, chemical shift $\delta = 5.32$), indicating four equivalent ptpy ligands per molecule with each ligand containing seven distinct aromatic protons. Proton resonances in the two ring systems "A" and "B"

Table III. ^{1}H NMR Assignments for ptpy and mppy Ir(III) Dimer and Monomer Complexes in CD_2Cl_2 (vs TMS)[a]

position	$[Ir(ptpy)_2Cl]_2$	$[Ir(mppy)_2Cl]_2$	$[Ir(ptpy)_2bpy]^+$	$[Ir(mppy)_2bpy]^+$
A_3	5.68 (s)	5.84 (d)	6.03 (s)	6.39 (d)
A_4		6.54 (t)		6.87 (m)
A_5	6.67 (d)	6.80 (t)	6.84 (m)	7.07 (m)
A_6	7.44 (d)	7.85 (d)	7.53 (m)	8.00 (d)
B_3	7.87 (d)		7.80 (d)	
B_4	7.76 (t)	7.61 (d)	7.66 (t)	7.57 (d)
B_5	6.79 (t)	6.70 (m)	6.84 (m)	6.87 (m)
B_6	9.21 (d)	9.29 (d)	7.36 (d)	7.50 (d)
C_3			9.25 (d)	9.19 (d)
C_4			8.13 (t)	8.22 (m)
C_5			7.36 (m)	7.42 (m)
C_6			7.90 (d)	7.86 (d)
Me	1.97 (s)	2.87 (s)	2.06 (s)	2.84 (s)

[a] Abbreviations: s, singlet; d, doublet; t, triplet; m, multiplet.

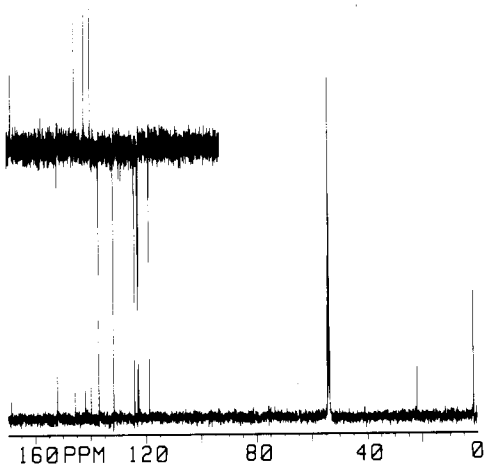

Figure 5. ^{13}C and APT (inset) NMR spectra for $[Ir(ptpy)_2Cl]_2$ in CD_2Cl_2 (GN-500 FT-NMR).

(Figure 1a,b) were assigned by 2D-COSY *J*-correlation connective analysis (Figure 4, inset).[27-29] The proton assignments are compiled in Table III. Proton assignments for $[Ir(mppy)_2Cl]_2$ and $[Ir(ptpy)_2Cl]_2$ are consistent with those assigned previously for the nonsubstituted $[Ir(ppy)_2Cl]_2$ dimer.[19,23,25,27,30-36]

The $[Ir(ptpy)_2Cl]_2$ (Figure 5) and $[Ir(mppy)_2Cl]_2$ ^{13}C NMR spectra resolved all 12 carbon resonances. The intensities of these signals are consistent with an aliphatic carbon ($\delta \approx 22$) and 11 aromatic carbons (four nonprotonated, seven protonated). The APT spectra for $[Ir(ptpy)_2Cl]_2$ (Figure 5, inset) and $[Ir(mppy)_2Cl]_2$ are supportive of this observation. The ^{13}C chemical shifts are compiled in Table IV, with the dichloromethane-d_2 solvent signal recorded at 53.8 ppm. Owing to the complexity of the spectra, the carbon resonances are not assigned.

3. Cyclic Voltammetry. Cyclic voltammetric measurements are illustrated by the four curves A–D in Figure 6. Curve A represents the voltammogram for the solvent–electrolyte solution,

Table IV. ^{13}C NMR Chemical Shifts for ptpy and mppy Ir(III) Dimer and Monomer Complexes in CD_2Cl_2 (vs TMS)[a]

$[Ir(ptpy)_2Cl]_2$	$[Ir(mppy)_2Cl]_2$	$[Ir(ptpy)_2bpy]^+$	$[Ir(mppy)_2bpy]^+$
168.4 (w)	166.4 (w)	168.1 (w)	166.1 (w)
151.8 (s)	151.0 (s)	156.4 (w)	156.2 (w)
145.4 (w)	147.4 (w)	150.8 (W)	152.3 (w)
141.8 (w)	146.6 (w)	150.7/150.5 (D)	150.4/150.2 (D)
139.6 (w)	141.3 (s)	148.8/148.6 (D)	147.4/147.2 (D)
136.8 (s)	132.1 (w)	141.4 (W)	145.9 (w)
131.5 (s)	131.0 (s)	140.1/138.9 (D)	142.5/142.3 (D)
123.9 (s)	128.4 (s)	138.4/138.2 (D)	140.1/139.9 (D)
122.7 (s)	128.2 (s)	132.9/132.5 (D)	133.4 (w)
122.4 (s)	122.6 (s)	128.5/128.2 (D)	132.1/131.8 (D)
118.6 (s)	121.4 (s)	126.6 (s)	130.0/129.7 (D)
21.7 (Me)	23.8 (Me)	125.2/125.0 (D)	129.3/129.1 (D)
		124.1/123.8 (D)	128.4/128.2 (D)
		123.2/122.9 (D)	126.5 (s)
		119.9/119.8 (D)	123.0/122.7 (D)
		119.8/119.7 (D)	122.6/122.4 (D)
		21.8 (Me)	23.9 (Me)

[a] CD_2Cl_2 solvent, $\delta = 53.8$. Abbreviations: w, weak signal, positive phase in APT, nonprotonated carbons; s, strong signal, positive phase in APT; D, doublet in SFORD, negative phase in APT, protonated carbons; Me, methyl carbons.

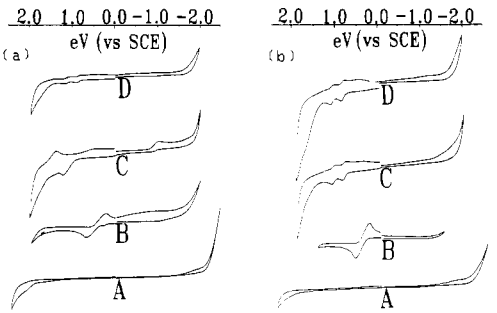

Figure 6. Cyclic voltammograms for methyl-substituted phenylpyridine Ir(III) dimer complexes (in CH_2Cl_2–TEAH at room temperature (vs SCE)) (a) $[Ir(ptpy)_2Cl]_2$ and (b) $[Ir(mppy)_2Cl]_2$: (A) solvent–TEAH CV scan; (B) internal reference CV scan, $Fc^{+/0}$; (C) CV scan of complex under repetitive scan; (D) CV scan of complex under single scan.

curve B represents the voltammogram for the $Fc^{+/0}$ reference, and curves C and D represent the voltammograms for the complex from two scanning techniques. Curve C measures the oxidative (or reductive) region by scanning between 0 and ±2.0 V (vs SCE) repetitively before voltammogram measurements. This curve is referred to as the "repetitive scan" curve. Curve D measures the oxidative (or reductive) region by measuring the voltammogram without prior repetitive scanning. This is referred to as the "single scan" curve.

Cyclic voltammograms of $[Ir(ptpy)_2Cl]_2$ in dichloromethane at room temperature with TEAH supporting electrolyte are shown in Figure 6a. Figure 6b shows the analogous CV measurements for the $[Ir(mppy)_2Cl]_2$ dimer. The single-scan voltammograms for these complexes show two reversible oxidative waves, $E_{1/2} \approx$

(27) Reveco, P.; Medley, J.; Garber, A. R.; Bhacca, N. S.; Selbin, J. *Inorg. Chem.* **1985**, *24*, 1096.
(28) Reveco, P.; Cherry, W. R.; Medley, J.; Garber, A.; Gale, R. J.; Selbin, J. *Inorg. Chem.* **1986**, *25*, 1842.
(29) Derome, A. E. In *Modern NMR Techniques for Chemistry Research*; Baldwin, J. E., Ed.; Pergamon: Oxford, U.K., 1986.
(30) Nanoyama, M. *Bull. Chem. Soc. Jpn.* **1979**, *52*(12), 3749.
(31) Kahl, J. L.; Hanck, K.; DeArmond, K. *J. Inorg. Nucl. Chem.* **1979**, *41*, 495.
(32) Gutierrez, M. A.; Newkome, G. R.; Selbin, J. *J. Organomet. Chem.* **1980**, *202*, 341.
(33) Spellane, P. J. Ph.D. Thesis, University of California, Santa Barbara, CA, 1985.
(34) Spellane, P. J.; Watts, R. J. *Inorg. Chem.* **1983**, *22*, 4060.
(35) Mader, U.; Jenny, T.; Zelewsky, A.-V. *Helv. Chim. Acta* **1986**, *69*, 1085.
(36) DeSimone, R. E.; Drago, R. S. *Inorg. Chem.* **1969**, *8*(11), 2517.

Table V. Cyclic Voltammetric Potentials for Ir(III) Dimer[a] and Monomer[b] Complexes (V vs SCE)

	E_{p_a}	E_{p_c}	$E_{p_a/2}$	$E_{p_c/2}$	E_{p-p}	$E_{1/2}$
			$[Ir(ppy)_2Cl]_2$			
oxidn scan, 1st[c]	0.96	0.83	0.90	0.95	0.13	0.93 (0.51)[d]
oxidn scan, 2nd	1.20	1.08	1.15	1.15	0.12	1.15 (0.73)
redn scan			no observable redn waves			
$Fc^{+/0}$	0.65	0.20	0.46	0.38	0.45	0.42
			$[Ir(ptpy)_2Cl]_2$			
oxidn scan, 1st	0.90	0.80	0.84	0.85	0.10	0.85 (0.39)
oxidn scan, 2nd	1.18	1.08	1.10	1.13	0.10	1.12 (0.66)
redn scan	−0.88	−1.00	−0.93	−0.90	0.12	−0.92 (−1.38)
$Fc^{+/0}$	0.70	0.24	0.58	0.34	0.46	0.46
			$[Ir(mppy)_2Cl]_2$			
oxidn scan, 1st	0.90	0.83	0.85	0.85	0.07	0.85 (0.41)
oxidn scan, 2nd	1.15	1.08	1.10	1.10	0.07	1.10 (0.66)
redn scan		−1.13		−1.00		
$Fc^{+/0}$	0.60	0.28	0.45	0.43	0.32	0.44
			$[Ir(ppy)_2bpy]^+$			
oxidn scan	1.32	1.24	1.12	1.20	0.08	1.28 (0.88)
redn scan	−1.34	−1.42	−1.37	−1.35	0.08	−1.38 (−1.78)
			$[Ir(ptpy)_2bpy]^+$			
oxidn scan, 1st	0.95					
oxidn scan, 2nd	1.20	1.18	1.15	1.20	0.02	1.18 (0.79)
redn scan	−1.40	−1.45	−1.43	−1.41	0.05	−1.42 (−1.81)
$Fc^{+/0}$	0.51	0.28	0.40	0.38	0.23	0.39
			$[Ir(mppy)_2bpy]^+$			
oxidn scan, 1st	1.05		1.01			
oxidn scan, 2nd	1.25	1.18	1.19	1.23	0.07	1.21 (0.81)
redn scan	−1.36	−1.45	−1.41	−1.40	0.09	−1.41 (−1.81)
$Fc^{+/0}$	0.50	0.29	0.40	0.40	0.21	0.40

[a] Solvent dichloromethane. [b] Solvent acetonitrile. [c] First (second) wave of oxidative or reductive scan. [d] Values in parentheses are $E_{1/2}$ vs $Fc^{+/0}$.

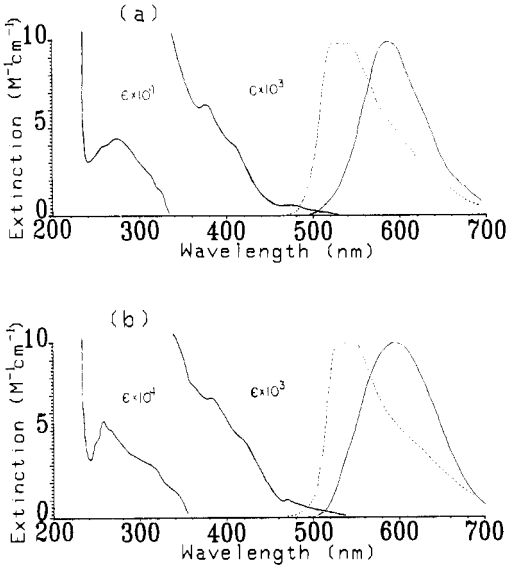

Figure 7. Absorption and emission measurements for Ir(III) monomer complexes (a) $[Ir(ptpy)_2bpy]^+$ and (b) $[Ir(mppy)_2bpy]^+$: (—) absorption and emission at room temperature in CH_2Cl_2; (---) emission at 77 K in EtOH–MeOH (4:1 v/v).

0.85, 1.11 V, and a weak reductive wave, $E_{p_c/2} \approx -0.95$ V versus SCE. The repetitive-scan voltammogram curves, however, show reversible oxidative behavior in the CV's of the mppy dimer but irreversible behavior in the CV's of the ptpy dimer. Redox potentials for these complexes are tabulated in Table V together with the $Fc^{+/0}$ reference potentials, $E_{1/2} \approx 0.45$ V versus SCE.

B. Iridium Monomers. 1. Absorption and Emission Properties. Absorption maxima for $[Ir(ptpy)_2bpy]^+$ and $[Ir(mppy)_2bpy]^+$ in dichloromethane (Figure 7) are compiled in Table I. The absorption profiles follow Beer's law in the concentration between

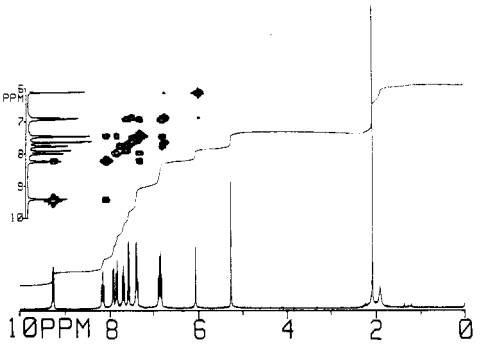

Figure 8. ^1H and 2D-COSY (inset) NMR spectra for $[Ir(ptpy)_2bpy]^+$ in CD_2Cl_2.

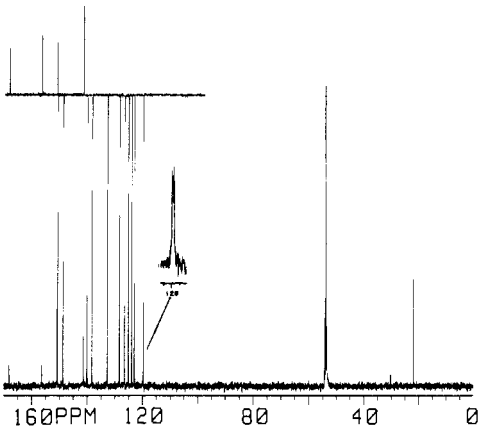

Figure 9. ^{13}C and APT (inset) NMR spectra for $[Ir(ptpy)_2bpy]^+$ in CD_2Cl_2 (SFORD for 120 ppm signal).

10^{-4} and 10^{-6} M. Ambient- and low-temperature (77 K, glasses) emission maxima for $[Ir(ptpy)_2bpy]^+$ and $[Ir(mppy)_2bpy]^+$ (Figure 7) are tabulated in Table II. The emission spectra for both methyl-substituted monomers are similar to that of the nonsubstituted ppy monomer,[18,26] showing broad profiles centered at 595 nm under ambient conditions and structured profiles with maxima near 527 and 550 nm under 77 K conditions. Room-temperature luminescence lifetimes for freeze–pump–thawed samples of $[Ir(ptpy)_2bpy]^+$ and $[Ir(mppy)_2bpy]^+$ in acetonitrile are 248 and 200 ns, respectively. Lifetimes in EtOH–MeOH (4:1 v/v) 77 K glasses are 1 order of magnitude longer at 4.93 and 4.38 μs, respectively (Table II).

2. ^1H and ^{13}C NMR Spectra. The monomer ^1H NMR spectra were more highly resolved in dichloromethane-d_2 than in any other solvent used; therefore, the NMR measurements were obtained using this solvent. The $[Ir(ptpy)_2bpy]^+$ (Figure 8) and $[Ir(mppy)_2bpy]^+$ ^1H NMR spectra in dichloromethane-d_2 feature 11 aromatic signals, and the contours in the COSY spectra (inset) suggest a three-ring system corresponding to rings "A", "B", and "C" (Figures 1 and 2b). Proton resonances were assigned by using *J*-correlation connective analysis on the 2D-COSY spectra (Table III).

The $[Ir(ptpy)_2bpy]^+$ (Figure 9) and $[Ir(mppy)_2bpy]^+$ ^{13}C NMR spectra show 15 aromatic resonances and one aliphatic resonance (Table IV). The SFORD spectra show complicated splitting patterns for some of the resonances ($\delta \approx 150.7$, 119.8 for the ptpy monomer, $\delta \approx 122.6$ for the mppy monomer); as such, these signals are interpreted to be the superposition of resonances. Although the resolutions of the SFORD spectra make these signals hard to interpret, we can account for 11 protonated and five nonprotonated carbon resonances by the phases of these signals in the APT spectra. No assignments were attempted for the ^{13}C NMR spectra.

3. Cyclic Voltammetry. The redox potentials for $[Ir(ptpy)_2bpy]^+$ and $[Ir(mppy)_2bpy]^+$ in acetonitrile with TEAH supporting electrolyte at room temperature are tabulated in Table V. The CV measurements for each monomer are illustrated by the four curves A–D in Figure 10, analogous to the dimer volt-

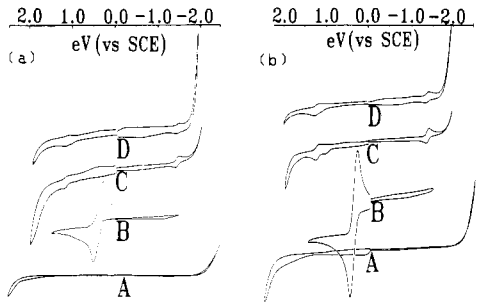

Figure 10. Cyclic voltammograms for methyl-substituted phenylpyridine Ir(III) monomer complexes (in acetonitrile–TEAH at room temperature (vs SCE)) (a) $[Ir(ptpy)_2bpy]^+$ and (b) $[Ir(mppy)_2bpy]^+$: (A) solvent–TEAH CV scan; (B) internal reference CV scan, $Fc^{+/0}$; (C) CV scan of complex under repetitive scan; (D) CV scan of complex under single scan.

ammograms. Both complexes show invariant redox patterns for repetitive and single scans, curves C and D, respectively. These voltammograms show two oxidative waves and a single reduction wave with only the second oxidative wave at $E_{1/2}$ = 1.20 V and the reductive wave at $E_{1/2}$ = −1.41 V versus SCE showing reversible behavior. In curves B of Figure 10, the potentials for the $Fc^{+/0}$ couple, $E_{1/2}$ = 0.40 V versus SCE, are shown.

IV. Discussion

A. Structural Considerations. The simplicity of the ^1H NMR spectra, with eight distinct resonances, suggests one "type" of NC ligand in each of the dimers (Figure 2a); thus, D_2 symmetry is assigned to the dimer structures.

These dimers react readily with the chelating 2,2′-bipyridine under mild conditions to form the $[Ir(NC)_2NN]Cl$ monomer with yields in excess of 90%. The mild synthetic conditions probably prevent bonding isomerization of the NC ligands to the iridium center, giving rise to monomeric complexes with the Ir–C bonds cis to each other (Figure 2b). In such a structure, the two ortho-metalating ligands in the complex, i.e., ptpy and mppy, are equivalent to each other as are the pyridyl halves in bipyridine as evidenced by the 11 aromatic resonances in the ^1H NMR spectra of the monomers.

The ^1H NMR and 2D-COSY spectra for $[Ir(ptpy)_2Cl]_2$ (Figure 4, Table III), suggest a two-ring system with coupled groups of two and four spins corresponding to the tolyl "A" and pyridyl "B" rings, respectively (Figure 1a). The uncoupled 5.7 ppm resonance is assigned to the isolated tolyl proton at the A_3 position in agreement with the nonsubstituted $[Ir(ppy)_2Cl]_2$ dimer assignment.[25,33] The two remaining tolyl signals are assigned to the A_5 and A_6 protons, with the lower field 7.4 ppm signal assigned to the proton ortho to the bridgehead carbons (A_6);[19,23,25,27,28,30-34] the additional tolyl signal at 6.7 ppm is thus assigned to the A_5 protons. The pyridyl protons are assigned to the remaining four signals at 9.2, 7.9, 7.8, and 6.8 ppm with the lowest field doublet assigned to the B_6 protons because of their juxtaposition over the bridging chlorides, a deshielded region of electron density (Figure 2a). This initial assignment of the B_6 resonance allows for J-correlation connective analysis of the B_6 9.2 ppm doublet to the B_5 6.8 ppm triplet, the B_5 6.8 ppm triplet to the B_4 7.8 ppm triplet, and the B_4 7.8 ppm triplet to the B_3 7.9 ppm doublet. It should be noted that the "ortho" B_3 resonance (protons ortho to the bridging carbon) is consistently assigned to the lower field resonance relative to either the B_4 or the B_5 resonance. Residual toluene is shown by the weak multiplet at 7.24 ppm, which is consistent with the elemental analysis.

The $[Ir(mppy)_2Cl]_2$ 2D-COSY spectrum indicates a two-ring system consisting of three coupled spins from the methylpyridyl "B" ring and four coupled spins from the phenyl "A" ring (Figure 1b). The A_3 and B_6 protons are assigned to the highest and lowest field signals at 5.8 and 9.3 ppm, respectively. These initial assignments provide for J-correlation connective analysis on the rest of the COSY spectrum. The resulting analysis is consistent with the low-field assignment of the ortho A_6 proton (δ = 7.85), relative to the meta A_5 (δ = 6.80) and para A_4 (δ = 6.54) protons. The sharp 2.87 ppm aliphatic singlet is assigned to the methyl protons, and residual toluene is observed as a multiplet at 7.2 ppm.

The carbon resonances in the ^{13}C NMR spectra[31,33,37-40] for $[Ir(ptpy)_2Cl]_2$ and $[Ir(mppy)_2Cl]_2$ (Table IV) were not assigned except for the isolated high-field methyl resonance $\delta \approx 22$ and the ortho-metalated carbon resonance $\delta \approx 141$, consistent with other metalated carbon resonances.[17,33,34,39] The $[Ir(ptpy)_2Cl]_2$ ^{13}C NMR spectrum in Figure 5 is representative of both dimers; the spectrum features seven intense and four weak signals in the aromatic region. The APT spectrum (inset) shows these signals as seven negative and four positive signals suggestive of seven protonated and four nonprotonated carbons. The simplicity of the ^{13}C NMR spectra, like that of the ^1H NMR spectra, supports a dimeric configuration with D_2 symmetry.

The ^1H NMR and 2D-COSY spectra for the $[Ir(ptpy)_2bpy]^+$ monomer are illustrated in Figure 8. J-correlation analysis on the COSY spectra elucidated three coupled groups consisting of "four", "three", and "four" spins, indicative of a symmetric monomer containing three unique rings. This is further substantiated by the one-proton-equivalent integration for each resonance in the aromatic region. These rings, labeled "A", "B", and "C" (Figures 1a,c and 2b), can be correlated to their appropriate coupled spins by using the methyl groups on the NC ligands as labels. The $[Ir(ptpy)_2bpy]^+$ 2D-COSY spectrum, for example, shows a three-coupled-spin system from the protons on the "A" tolyl NC rings, a four-coupled-spin system from the protons on the "B" pyridyl NC rings, and a four-coupled-spin system from the protons on the "C" pyridyl NN rings. In comparison, the methyl groups on the "B" pyridyl NC rings of the $[Ir(mppy)_2bpy]^+$ monomer lead to a three-coupled-spin system from the protons on the "B" methylpyridyl NC rings, a four-coupled-spin system from the protons on the "A" phenyl NC rings, and a four-coupled-spin system from the protons on the "C" pyridyl NN rings. These ring assignments support monomeric structures in which the halves of the two pyridyl rings in bpy form equivalent four-spin sets. Furthermore, if the lowest field resonances, δ = 9.25 for $[Ir(ptpy)_2bpy]^+$ and δ = 9.2 for $[Ir(mppy)_2bpy]^+$, are both assigned to protons on the pyridyl "C" rings, then the four coupled resonances from the "C" pyridyl "NN" rings may be distinguished from the other systems of four coupled resonances. It follows that the remaining system of four coupled spins is assigned to the pyridyl "B" rings of the ptpy ligands in the $[Ir(ptpy)_2bpy]^+$ ^1H NMR spectrum and to the phenyl "A" rings of the mppy ligands in the $[Ir(mppy)_2bpy]^+$ ^1H NMR spectrum.

Protons adjacent to the C–Ir and N–Ir bonds (C_6, B_6, and A_3 protons) are susceptible to shielding because of ring current perturbation from an adjacent ligand, thereby suggesting high-field assignments of these protons. Whereas the A_3 protons are shielded not only by the ring currents but also by the electron-rich Ir–C moiety, the B_6 and C_6 protons are deshielded by an adjacent electronegative nitrogen atom, which offsets the shielding effect from the ring current. This facilitates assignment of the B_6 and C_6 proton resonances to the middle of the aromatic region at δ = 7.4 and 7.9, respectively, and the A_3 proton resonance to the high-field aromatic region at δ = 6.0. The lowest field resonance at 9.25 ppm is assigned to the C_3 protons due to their location ortho to a bridgehead carbon. Similarly, the "ortho" bridgehead A_6 and B_3 protons have low-field assignments at 7.5 and 7.8 ppm, respectively. With use of these initial assignments, it follows from J-correlation analysis that the superpositions of signals at 7.4 and 6.8 ppm, arising from protons in magnetically equivalent environments, are assigned to protons in the B_6, C_5 and A_5, B_5 positions. Finally, the methyl protons are unambiguously assigned to the 2.1 ppm sharp singlet. Proton assignments are compiled in Table III.

(37) Farver, O.; Monsted, O.; Nord, G. *J. Am. Chem. Soc.* **1979**, *101*(20), 6118.
(38) Lavallee, D. K.; Baughman, M. D.; Phillips, M. P. *J. Am. Chem. Soc.* **1977**, *99*(3), 718.
(39) Garber, A. R.; Garrou, P. E.; Hartwell, G. E.; Smas, M. J.; Wilkinson, J. R.; Todd, L. J. *J. Organomet. Chem.* **1975**, *86*, 219.
(40) Steel, P. J.; LaHousse, F.; Lerner, D.; Marzin, C. *Inorg. Chem.* **1983**, *22*, 1488.

The ^1H NMR assignments for $[Ir(mppy)_2bpy]^+$ are also compiled in Table III. The proton contours from the COSY spectrum are assigned by using the same strategy used for the proton contours of the $[Ir(ptpy)_2bpy]^+$ COSY spectrum, with the A_3, B_6, and C_6 protons again assigned to high-field resonances because of their spatial orientation with the A_3 proton assigned the highest field signal because of the added shielding from the adjacent electron-rich Ir–C moiety. The ortho bridgehead C_3 and A_6 protons are assigned to lowest field resonances, with respect to their ring systems, for the reasons stated above. The signal from the B_3 protons is absent in this spectrum.

The ^{13}C NMR and APT spectra for the $[Ir(ptpy)_2bpy]^+$ monomers resolved only 15 of the 16 carbon resonances (Figure 9). Using intensity information from the ^{13}C spectrum, splitting patterns from the carbon spectrum, and phase information from the APT spectrum, we can account for four protonated carbons and 11 nonprotonated carbons. In the SFORD spectrum (Figure 9, inset), however, the resonance at $\delta = 119.8$ shows a complicated splitting pattern. If we interpret this signal to be the superposition of two carbon resonances, one nonprotonated and the other protonated, than all five protonated carbons and 11 nonprotonated carbons are observed. The complexity of the ^{13}C spectrum arises from the overlap of signals in the aromatic region as described by Marker.[41] The resonance at $\delta = 141.4$ is interpreted as the resonance arising from the ortho-metalated carbon. Other than the methyl carbon assignment, $\delta = 21.8$, no additional assignments were attempted for the ^{13}C NMR spectra. The chemical shifts for the carbon nuclei are compiled in Table IV.

The ^{13}C NMR spectra for $[Ir(mppy)_2bpy]^+$ resolved all 11 protonated carbons and five nonprotonated carbons. The resonance at $\delta = 145.9$ is interpreted as the ortho-metalated carbon resonance, and the aliphatic resonance at $\delta = 23.9$ is assigned to the methyl carbon resonance. Carbon resonances are compiled in Table IV.

In general, the resonances from the tolyl "A" rings in the ptpy dimer and monomer are higher field relative to the resonances from the phenyl "A" rings in the mppy dimer and monomer because of the inductive perturbation from the methyl groups.[27,28,42,43] Similarly, the signals from the methylpyridyl "B" rings in the mppy complexes are higher field relative to those from the pyridyl "B" rings in the ptpy complexes. If one views these ortho-metalating ligands as both strong σ-donors via the phenyl or tolyl "A" ring systems and good π-acceptors through the pyridyl or methylpyridyl "B" rings, then the chemical shift information may be taken to indicate that the ptpy ligand is both a better σ-donor and a stronger π-acceptor than the mppy ligand.

Several structural conclusions can be drawn from the chemical shift patterns. As mentioned previously, the symmetry of these molecules can be deduced from the simplicity of the NMR spectra. The question arises, however, as to whether the ortho-metalating carbons or the chelating nitrogens occupy the axial positions. It has been argued that the dimeric structure possesses two mutually trans Ir–N bonds and two mutually cis Ir–C bonds trans to the bridging chlorides;[25] chemical shifts from the A_3 and B_6 protons support this contention. The fact that in the dimer the A_3 protons are the highest field resonance and the B_6 protons are the lowest field resonance indicates that the ligands are aligned in a fashion which places the A_3 protons in a chemically shielded environment and the B_6 protons in a chemically deshielded environment. Such a position can only occur if the carbons are mutually cis to each other and trans to the bridging chlorides as shown in Figure 2a. Recent X-ray crystal structures of both $[Rh(ppy)_2Cl]_2$ and $[Ir(ptpy)_2Cl]_2$ support such a conformation.[44,45]

B. Photophysical Assignment. The absorption features for the $[Ir(ptpy)_2Cl]_2$ and $[Ir(mppy)_2Cl]_2$ dimers in dichloromethane (Figure 3) are similar to those of $[Ir(ppy)_2Cl]_2$,[25] displaying band maxima near 483, 434, and 400 nm. Similarly, the absorption features for the $[Ir(ptpy)_2bpy]^+$ and $[Ir(mppy)_2bpy]^+$ monomers (Figure 7) resemble those of $[Ir(ppy)_2bpy]^{2+}$.[18,26,46] Absorption maxima for the monomers are seen around 467, 414, 381, and 335 nm with π–π^* transitions around 270 and 256 nm. The low-energy bands between 480 and 300 nm for both monomeric and dimeric complexes are assigned to MLCT transitions as evident from their hypsochromic shifts in polar solvents.[47,48] The methyl groups in these substituted complexes have only small effects on the energies of the charge-transfer absorption bands as evident from the band maximum similarities in the absorption profiles. Changes of the low-energy band are difficult to monitor because of the low resolution of the absorption features caused by the overlap of several bands (Figures 3 and 7). The small differences in the low-energy band maxima can be explained, however, by considering the opposing effects of methyl substituents on the σ-donor and π-acceptor abilities of phenylpyridine. The electron density at the metal is presumed to be enriched by methyl substitution through the σ-bonding framework, while the ligand's π-acceptor ability may be reduced in a corresponding manner. The net result is a very small effect on the spectroscopic metal-to-ligand charge-transfer energies as is observed in the absorption maxima of these complexes.

The room-temperature emission spectra for the $[Ir(ppy)_2Cl]_2$ and $[Ir(mppy)_2Cl]_2$ dimers show a single broad emission feature near 515 nm. However, the $[Ir(ptpy)_2Cl]_2$ dimer displays both the 515-nm emission band as well as a second band at 580 nm. Two findings suggest that this second band arises from a monomer solvento complex in thermal equilibrium with the $[Ir(ptpy)_2Cl]_2$ dimer. First, the 580-nm emission band maximum is very near that of the bpy-substituted monomers, and second, preliminary work in neat dichloromethane with variable-temperature emission spectroscopy shows that this feature collapses at low temperatures (77–200 K) but develops at higher temperatures (250–300 K), suggesting that at low temperatures dimer formation is favored but at elevated temperatures thermal cleavage is promoted.

Emission spectra for the dimers in 77 K glasses (Figure 3) show structured emission profiles centered around 483–497 and 526–530 nm. A trend follows in which the nonsubstituted $[Ir(ppy)_2Cl]_2$ dimer[25,46] has the highest energy emissive features (483, 525 nm), followed by $[Ir(ptpy)_2Cl]_2$ (490, 526 nm) and, finally, the $[Ir(mppy)_2Cl]_2$ dimer (497, 530 nm). The relative emission energies from these spectroscopic measurements suggest that the activating methyl on the NC ligands facilitate the lowest energy metal-to-ligand charge-transfer transitions. Lifetimes of 5 μs for the dimers and monomers in 77 K glasses support MLCT assignments of these low-energy emission bands.

The room-temperature emission spectra for the methyl-substituted $[Ir(NC)_2bpy]^+$ monomers (Figure 7) show broad structureless bands in dichloromethane but modest emission structure in 77 K MeOH–EtOH–DCM (4:1:1 v/v) glasses. Preliminary results from variable-temperature excitation–emission measurements suggest that these bands originate from the dual emission of the MLCT states associated with the ortho-metalating (NC) and chelating (bpy) ligands.[18,26,46] Work is currently in progress to time-resolve these emission features.

C. Electrochemical Properties. Cyclic voltammograms for $[Ir(ptpy)_2Cl]_2$ (Figure 6a) under single-scan conditions show two reversible oxidative waves at $E_{1/2} = 0.85$ and 1.12 V and a weak reductive wave at $E_{1/2} = -0.92$ V (Table V). Under repetitive-scan conditions, however, the oxidative voltammograms indicate a two-electron irreversible process and the reductive voltammograms show current ratios of $I_c/I_a \approx 2$. The deformation of these waves

(41) Marker, A.; Canty, A. J.; Brownlee, R. T. C. *Aust. J. Chem.* **1978**, *31*, 1255.
(42) Fabian, R. H.; Klassen, D. M.; Sonntag, R. W. *Inorg. Chem.* **1980**, *19*, 1977.
(43) Vila, J. M.; Pereira, M. T.; Suarez, A.; Gayoso, E.; Gayoso, M. *Synth. React. Inorg. Met.-Org. Chem.* **1986**, *16*(4), 499.
(44) Sprouse, S. D. Ph.D. Thesis, University of California, Santa Barbara, CA, 1984.
(45) Garces, F.; Watts, R. J., unpublished results.
(46) King, K. A. Ph.D. Thesis, University of California, Santa Barbara, CA, 1986.
(47) Turro, N. J. *Modern Molecular Photochemistry*; Benjamin/Cummings: Menlo Park, CA, 1978.
(48) Drago, R. S. *Physical Methods in Chemistry*; W. B. Saunders: Philadelphia, PA, 1977.

Table VI. Redox Potentials for Ir(III) Dimer and Monomer Complexes (vs $Fc^{+/0}$)

complex	emissn E_a	$E(ox)_{1/2}$ $E(2+/+)$	$E(red)_{1/2}$ $E(+/0)$	photoredox $E(2+/*+)$	photoredox $E(*+/0)$
$[Ir(ppy)_2Cl]_2$	2.57 (483)	0.51		−2.06	
$[Ir(ptpy)_2Cl]_2$	2.53 (490)	0.39	−1.38	−2.14	
$[Ir(mppy)_2Cl]_2$	2.49 (497)	0.41		−2.08	
$[Ir(ppy)_2bpy]^+$	2.33 (532)	0.88	−1.78	−1.45	0.55
$[Ir(ptpy)_2bpy]^+$	2.37 (526)	0.79	−1.81	−1.58	0.56
$[Ir(mppy)_2bpy]^+$	2.35 (528)	0.81	−1.81	−1.54	0.54

[a] Values in parentheses are emission maxima (nm) at 77 K (see Table II).

suggests dimer instability under these conditions.[49] On the other hand, cyclic voltammograms for $[Ir(mppy)_2Cl]_2$ under single- and repetitive-scan conditions (Figure 6b) show identical wave patterns consisting of two reversible oxidative waves at $E_{1/2}$ = 0.85 and 1.10 V and a very weak irreversible reductive wave at $E_{p_c/2}$ = −1.00 V (Table V). The invariant oxidative patterns shown for the two scan modes for this dimer suggest stable oxidized Ir(III)/Ir(IV) and Ir(IV)/Ir(IV) dimeric species. The weak reduction current seen in the CV's for both dimers suggests that the methyl-substituted dimers undergo some reduction with the $[Ir(ptpy)_2Cl]_2$ dimer displaying lower reductive potential (E_{p_c}) by 110 mV over that of the $[Ir(mppy)_2Cl]_2$ dimer. Previous studies of the parent complex[26] have indicated that reduction on the phenyl ring occurs at more negative potentials than reduction on the pyridyl ring since the electronegative nitrogen of the pyridyl ring serves to facilitate electroreduction whereas the excess negative charge in the metalated phenyl ring renders the metalated ring more difficult to reduce. Furthermore, ligand reduction in the methyl-substituted dimers occurs more readily on the aromatic ring without the methyl group because of the methyl's electron-donating influence.[50] The degree of reducibility for these dimers is consistent with initial reduction at the pyridyl ring of the NC ligand (Table V).[26,44,46]

The electrochemical data for the monomers show similar CV behavior (Figure 10, Table V). In general the methyl-substituted monomer complexes are better behaved than their dimer counterparts, giving single reversible oxidative and reductive waves. Two conclusions can be drawn from the redox potentials of the monomer complexes. First, the lower oxidative potential for $[Ir(ptpy)_2bpy]^+$ ($E_{1/2}$ = 1.18 V) over that of $[Ir(mppy)_2bpy]^+$ ($E_{1/2}$ = 1.21 V) by 30 mV suggests that the iridium of the ptpy monomer possesses higher charge density, which is in good agreement with other spectroscopic data. Second, the identical reduction potentials ($E_{1/2}$ = −1.41 V) for these monomers suggest that the reduction occurs on the bipyridine ligand and is independent of the charge density on the iridium center.[18,26,46] These observations suggest localized reduction of the bipyridine ligand in these monomers. No additional reductive features were observed up to potentials of −2.5 V (vs SCE), the limit of the solvent window under dry-ice temperatures.

When the redox potentials are corrected by the internal reference $Fc^{+/0}$, the oxidative potentials for the methyl-substituted dimers (under reversible conditions) are lower than those of the nonsubstituted ppy dimers by 100 mV for the first oxidative wave and by 70 mV for the second oxidative wave. Similarly, the methyl-substituted monomers are easier to oxidize and harder to reduce than the ppy monomer by 90 and 30 mV, respectively. In the literature, chelated polypyridyl complexes containing functional groups such as carboxylic acids, diethyl esters, and methyls on bipyridine exhibit only a 30-mV anodic enhancement relative to their nonsubstituted counterparts.[51-55] The greater enhancement of the anodic potentials for the methyl-substituted complexes of the ortho-metalated complexes studied here suggests that the methyls influence the electron density on the metal in these ppy complexes to a greater extent than do methyls on chelating ligands such as bipyridine.

V. Summary

Ir(III) complexes with methyl-substituted ppy ligands possess higher electron density about the metal center than do their nonsubstituted parent complexes. This increase in electron density is demonstrated by the shielding enhancement in the NMR chemical shifts of the nuclei of the ring system containing the methyl group and by the cathodic shifts of the oxidative and reductive potentials from the CV measurements. In good agreement with the CV results, absorption–emission data indicate competing σ-donor and π-acceptor effects from the methyl groups during charge-transfer processes. That is, although MLCT transitions are facilitated by the added electron density on the metal, the poorer π-accepting ability of the methyl-substituted ligands renders charge transfer more difficult. As a result, transitions occur at energies similar to those of the nonsubstituted ppy complexes.

From the electrochemical and spectroscopic data, Table VI is constructed. This table indicates that methyl groups on the ppy ligand of ortho-metalated monomer complexes enhance the photoredox potential, $E(2+/*+)$, of the low-energy state by as much as 100 mV over that of their nonsubstituted counterpart. The results from this study indicate that the electron density about the iridium metal and, consequently, the reducing power of Ir(III) phenylpyridine ortho-metalated complexes are enhanced via structural modification of the ligand, thereby creating a stronger photoreducing agent.

Acknowledgment. This work was supported by the Office of Basic Energy Sciences, United States Department of Energy, Project DE-AT03-78ER70277. F.O.G. was supported by a UCSB Campus Fellowship, 1984–1987.

(49) Brown, E. R.; Large, R. F. *Electrochemical Methods*; Physical Methods of Chemistry IIA; Wiley-Interscience: New York, 1971.
(50) Dose, E. V.; Wilson, L. J. *Inorg. Chem.* **1978**, *17*, 2660.
(51) Saji, T.; Aoyagui, S. *J. Electroanal. Chem. Interfacial Electrochem.* **1975**, *60*, 1.
(52) Gaines, G. L., Jr.; Behnken, P. E.; Valenty, S. J. *J. Am. Chem. Soc.* **1978**, *100*, 6547.
(53) Ferguson, J.; Mau, A. W.-H.; Sasse, W. H. F. *Chem. Phys. Lett.* **1979**, *68*(1), 21.
(54) Constable, E. C.; Holmes, J. M. *J. Organomet. Chem.* **1981**, *214*, 253.
(55) Donohoe, R. J.; Tait, C. D.; DeArmond, M. K. *J. Phys. Chem.* **1986**, *90*, 3923.